JOURNAL OF GEOPHYSICAL RESEARCH, VOL. 114, A08204, doi:10.1029/2009JA014194, 2009

Plasmaspheric dynamics resulting from the Hallowe'en 2003 geomagnetic storms

Z. C. Kale,[1] I. R. Mann,[1] C. L. Waters,[2] M. Vellante,[3] T. L. Zhang,[4] and F. Honary[5]

Received 27 February 2009; revised 1 May 2009; accepted 28 May 2009; published 11 August 2009.

[1] Cross-phase-derived plasma mass density trends during the Hallowe'en 2003 geomagnetic storms are presented for $38° \lesssim$ magnetic latitude $\lesssim 63°$ ($1.61 \leq L \leq 5.10$), using data from the SAMNET (Subauroral Magnetometer Network), BGS (British Geological Survey), and SEGMA (South European Geomagnetic Array), ground-based magnetometer arrays in Europe. At all latitudes monitored, a rapid increase of total mass density is observed immediately following the initial storm sudden commencement at 0611 UT on 29 October, believed to be due to rapid ionospheric O^+ outflow. Plasmaspheric density depletion to at least 50° magnetic latitude ($L \sim 2.4$) took place over the next 3 days. Poststorm refilling began on 2 November. Following the sudden commencement of another storm on 4 November, a density enhancement was monitored at $2.79 \leq L \leq 3.84$, with subsequent plasmaspheric depletion occurring by 6 November. Plasma mass density values are compared to empirical plasmapause location model predictions, with reasonable agreement for most days, but density depletion and refilling were monitored 1 day after they are predicted. During poststorm plasmaspheric refilling, some extremely low early morning resonance frequencies are monitored and appear be due to quarter mode standing waves. This study also highlights that care must be taken in the choice of assumed geomagnetic field geometry when deriving plasma mass densities from observed field line resonances during severe geomagnetic storms.

Citation: Kale, Z. C., I. R. Mann, C. L. Waters, M. Vellante, T. L. Zhang, and F. Honary (2009), Plasmaspheric dynamics resulting from the Hallowe'en 2003 geomagnetic storms, *J. Geophys. Res.*, *114*, A08204, doi:10.1029/2009JA014194.

1. Introduction

[2] The plasmasphere is a region of near Earth space which typically extends from the ionosphere out to 4 R_E ($L \sim 4$) [e.g., *Baumjohann and Treumann*, 1999]. The plasmasphere particle properties and the location of its outer boundary, the plasmapause, are extremely dynamic, responding chiefly to changes in the dawn-dusk electric field caused by varying solar wind conditions. Under extreme storm-time conditions the plasmapause has been detected as close as $L \sim 2$ [e.g., *Chi et al.*, 2000]; while after an extended geomagnetically quiet interval the plasmasphere extends such that the plasmapause may not be apparent until $L \sim 8$ [e.g., *Carpenter and Anderson*, 1992].

[3] Plasmaspheric plasma is predominantly cold (~1 eV), and its major ionic constituent is H^+, with a smaller quantity of He^+ ($N(He^+)/N(H^+) \leq 0.3$ [e.g., *Lemaire et al.*, 1998, and references therein]). O^+ ions are also present, and typically $N(O^+)/N(H^+) \leq 0.1$ [e.g., *Comfort et al.*, 1988], but on occasion during active times this ratio may become close to unity [e.g., *Horwitz et al.*, 1984]. The behavior of these two heavy ion species is currently poorly understood but is an important consideration when interpreting plasma mass density profiles [e.g., *Menk et al.*, 2004; *Fraser et al.*, 2005]. Some studies have shown that an enhanced O^+ population may be present in the vicinity of the plasmapause following geomagnetic storms [e.g., *Horwitz et al.*, 1984; *Dent et al.*, 2006], however the frequency of occurrence and the conditions required to precipitate this effect this are unknown.

[4] Storm-time drainage of plasmaspheric plasma has been monitored for several decades, and recent IMAGE EUV images of the He^+ population have shown drainage plumes, or tails, extending out from the day-side plasmasphere toward the magnetopause [e.g., *Sandel et al.*, 2001; *Goldstein et al.*, 2003; *Sandel et al.*, 2003]. The time taken for a flux tube to reach a density minima, which could be considered to represent the beginning of the refilling process, is difficult to determine, hindering a better understanding of the processes controlling the rate of plasma drainage.

[5] This paper presents a ground-based survey of observed geomagnetic field line resonance frequencies and the resulting equatorial plasma mass densities which are derived from those frequencies. Specifically, the field line

[1]Department of Physics, University of Alberta, Edmonton, Alberta, Canada.
[2]School of Mathematical and Physical Sciences, University of Newcastle, Callaghan, New South Wales, Australia.
[3]Dipartimento di Fisica, Università dell'Aquila, L'Aquila, Italy.
[4]Space Research Institute, Austrian Academy of Sciences, Graz, Austria.
[5]Department of Communication Systems, University of Lancaster, Lancaster, UK.

0148-0227/09/2009JA014194$09.00

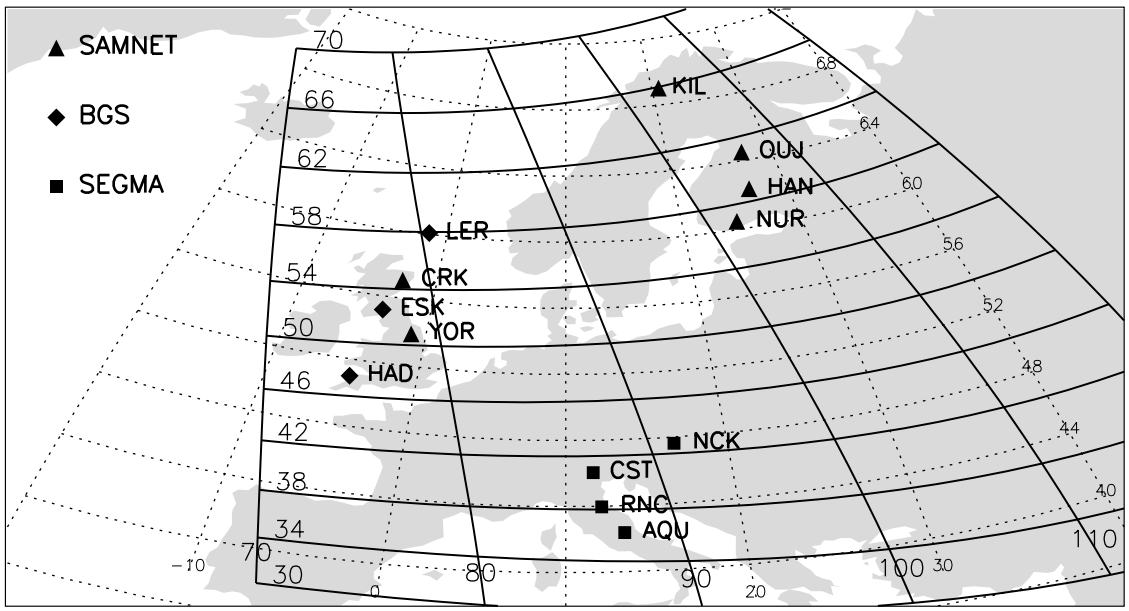

Figure 1. Locations of the ground-based magnetometers employed. Solid grid shows magnetic latitudes and longitudes; dotted grid shows geographic latitudes and longitudes.

resonance frequency and plasma mass density values for $38° \lesssim$ magnetic latitude $\lesssim 63°$, for the so-called "Hallowe'en" storms interval between 28 October and 6 November 2003 are examined as functions of Universal Time and field line location.

2. Data Analysis

[6] The cross-phase technique has been developed in order to allow a profile of field line resonance frequencies to be identified using arrays of latitudinally separated ground-based magnetometers [e.g., *Baransky et al.*, 1989; *Waters et al.*, 1991, 1994, 1995, and references therein]. The technique assumes that each field line is excited at its natural frequency, although the power at this frequency usually does not dominate the spectra, and may be at the level of the broadband background signal. The resonance occurs as a toroidal mode wave, i.e., monitored in the North-South, or, H-component ground-based geomagnetic field data after an assumed 90° polarization rotation upon transmission through the ionosphere [e.g., *Hughes*, 1974]. By comparing the H-component amplitude and phase spectra from two latitudinally separated ground-based magnetometer stations, the local field line resonance frequency may be identified, even though that frequency may not dominate the spectra. A resonance frequency is identified where a peak in phase difference (cross-phase) and a zero crossing, with negative gradient, of the amplitude difference occurs. This analysis is based on the expected 180° phase change, and amplitude peak through a resonance frequency. By examining all power ranges within the geomagnetic field data spectra, we are therefore able to construct a latitudinal profile of field line resonance frequencies, and monitor it as a function of time. For the cross-phase technique to be successful, pairs of stations must be sufficiently latitudinally separated that two distinct field line resonance frequencies occur, but the pair must be close enough that the signals are highly coherent.

[7] The natural field line resonance frequency of a flux tube depends on the length of that tube between the north and south ionospheres, the magnetic field strength, and the plasma mass density distribution along the field line. By assuming some geomagnetic field geometry and plasma density distribution, an observed latitudinal profile of resonance frequencies may be inverted in order to determine a plasma mass density profile in the equatorial plane. In the present study, the *Singer et al.* [1981] linearized wave equation was solved using a Tsyganenko 01 (T01 [*Tsyganenko*, 2002a, 2002b]) geomagnetic field model and assuming an inverse power law radial density variation along field lines, $\rho = \rho_{eq}(r/r_{eq})^{-m}$, with m = 3, where ρ (ρ_{eq}) and r (r_{eq}) are the density and radial distance along the field line (at the equator), respectively. *Menk et al.* [1999] found that the value of m can be highly variable, with values between 1 and 6, but that the chosen value is not critical for obtaining reliable estimates of the equatorial plasma mass density. For the current study, errors associated with cross-phase determined densities are estimated from the range of uncertainty associated with determining the field line resonance frequencies.

[8] Note that at lower magnetic latitudes ($\leq 45°$, $L \lesssim 2$), the use of a much steeper radial density variation may be more appropriate and a larger contribution to the eigenfrequency from the ionospheric density profile is expected [e.g., *Menk et al.*, 2000; *Poulter et al.*, 1984; *Vellante and Förster*, 2006]. A r^{-3} radial density distribution has been adopted at all magnetic latitudes studied for consistency, which may result in an overestimation of densities at the lower latitudes. Any overestimation is unlikely to affect the inferred day-to-day variations at the low L shells, and hence is unlikely to affect the overall conclusions from this study.

Table 1. Ground-Based Magnetometer Station Pairs Employed[a]

Station Pair	Geographic Latitude (°N)	Geographic Longitude (°E)	Magnetic Latitude (°N)	Magnetic Longitude (°E)	L Shell of Midpoint	MLT (CGM)	Separation (° Magnetic Latitude)
AQU-RNC	43.18	12.70	37.29	87.00	1.61	UT + 1h34	1.97
AQU-CST	44.22	12.49	38.58	87.03	1.67	UT + 1h34	4.55
RNC-CST	45.01	11.87	39.55	86.65	1.71	UT + 1h32	2.58
AQU-NCK	45.00	15.02	39.59	89.40	1.72	UT + 1h44	6.50
RNC-NCK	45.80	14.40	40.55	89.02	1.74	UT + 1h42	4.53
CST-NCK	46.84	14.19	41.80	89.07	1.83	UT + 1h42	1.95
HAD-YOR	52.47	357.24	49.24	76.55	2.39	UT + 0h43	3.30
YOR-CRK	55.52	358.16	52.79	78.39	2.79	UT + 0h10	3.80
ESK-LER	57.73	357.81	55.36	79.02	3.15	UT + 0h52	5.34
CRK-LER	58.61	358.09	56.34	79.64	3.32	UT + 0h55	3.33
NUR-HAN	61.40	25.65	57.84	103.46	3.60	UT + 2h50	1.83
NUR-OUJ	62.52	25.95	58.99	104.19	3.84	UT + 2h43	4.10
OUJ-KIL	66.77	24.01	63.45	104.84	5.10	UT + 2h45	4.88

[a]L shell, geomagnetic coordinates, and MLT calculated using the NSSDC MODELWeb facility (http://modelweb.gsfc.nasa.gov/models/cgm/cgm.html).

[9] The ground-based magnetometer data presented in this paper are from three arrays located in the European sector: SAMNET (Subauroral Magnetometer Network [e.g., *Yeoman et al.*, 1990, http://www.dcs.lancs.ac.uk/iono/samnet/]), BGS (British Geological Survey, data available from SAMNET) and SEGMA (South European Geomagnetic Array [*Villante et al.*, 2003; *Vellante et al.*, 2004, http://sole-terra.aquila.infn.it]). Figure 1 shows the locations of all of the magnetometers employed for this study. The station pairs employed for the cross-phase analysis presented in this paper are given in Table 1.

3. Results

[10] Figure 2 shows selected solar wind parameters monitored by the ACE satellite, and geomagnetic indices for 28 October to 6 November 2003. The sharp increase in solar wind bulk speed on 29 October resulted in a storm sudden

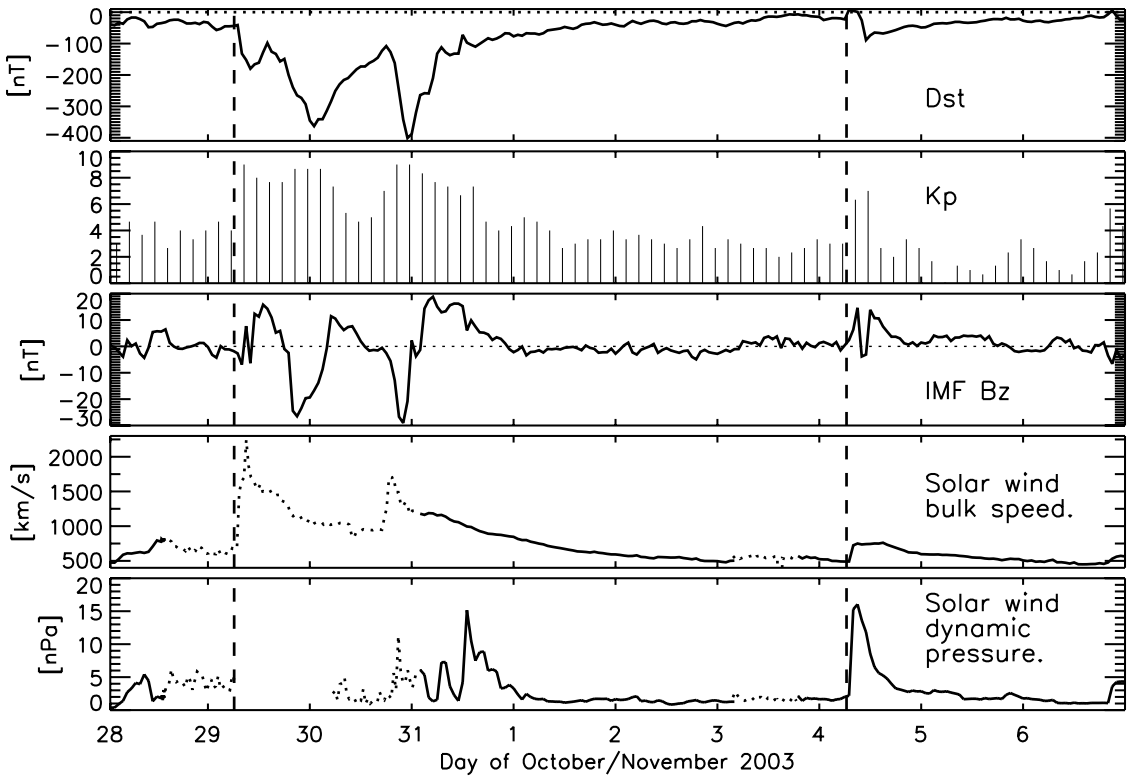

Figure 2. Kp, Dst, and ACE MAG (Magnetic Field Experiment) and SWEPAM (Solar Wind Electron, Proton, and Alpha Monitor) solar wind parameters as function of UT for 28 October–6 November 2003. A 1-hour delay has been included on the ACE data plots. ACE parameters are hourly averages, except in the regions denoted by dotted lines, which show higher resolution ACE SWEPAM data recovered by the ACE SWEPAM team [*Skoug et al.*, 2004]. Vertical dashed lines have been added at the times of the two storm sudden commencements occurring during this interval.

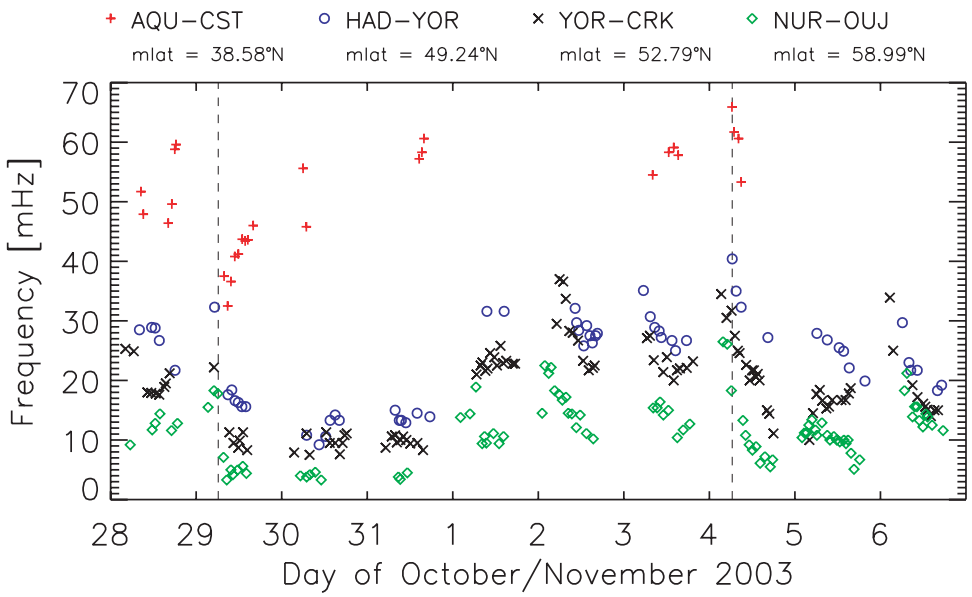

Figure 3. Cross-phase determined field-line resonance frequencies for four flux tubes for 28 October–6 November 2003 (AQU-CST, HAD-YOR, YOR-CRK, and NUR-OUJ). Dashed vertical lines have been placed at the UT of the two SSCs occurring during this interval.

commencement (SSC) at 0611 UT. Enhanced geomagnetic activity occurred until a minimum Dst value of −383 nT was monitored at 2300 UT on 30 October, after which storm time recovery commenced. During the most active period the solar wind reached speeds greater than 1000 km/s and the IMF B_Z (GSM coordinates) was strong and periodically northward and southward. The recovery phase, shown by the increasing Dst and decreasing Kp indices, continued until a second SSC took place at 0625 UT on 4 November. The resulting second disturbance was less intense and shorter lived in terms of Kp and Dst than that following the first SSC.

[11] Of the thirteen station pairs, four were chosen to monitor field line resonant frequency as a function of time throughout the study interval, while all thirteen were employed to produce daily profiles with good spatial resolution.

[12] Figure 3 shows the time variation of field line resonance frequencies as monitored by four magnetometer station pairs: AQU-CST, HAD-YOR, YOR-CRK and NUR-OUJ, with midpoints at northern magnetic latitudes (mlat) of 38.58°, 49.24°, 52.79° and 58.99°, respectively. These field line resonance frequency values were determined via the cross-phase technique, with Fourier transform data windows between 20 and 50 minutes duration. The higher frequencies appear at lower latitudes. For the HAD-YOR, YOR-CRK and NUR-OUJ pairs, the frequencies are lower for up to three days after the 0611 UT SSC, then increase

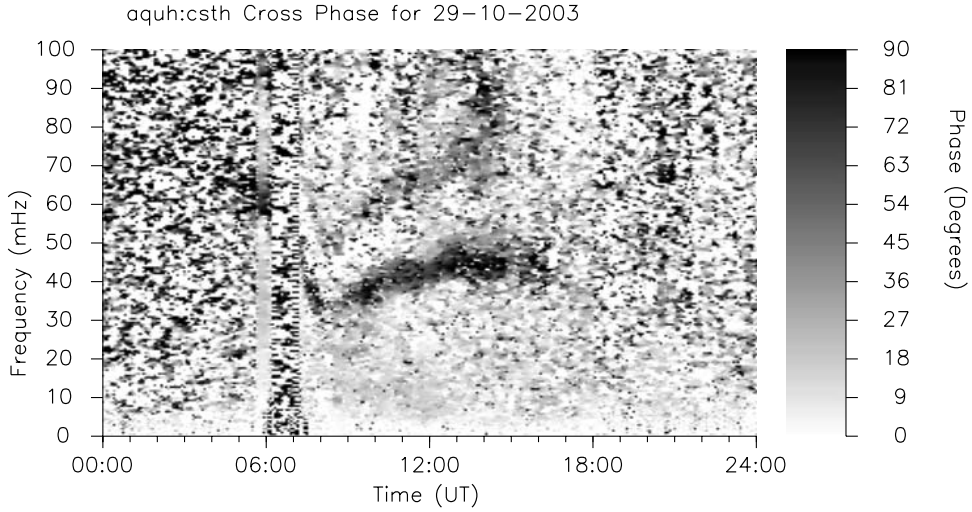

Figure 4. Dynamic cross-phase spectra for the AQU-CST station pair (magnetic latitude = 39°N) for 29 October 2003. A similar diurnal trend was shown in dynamic cross-phase spectra from all of the SEGMA station pairs (37°N ≤ magnetic latitude ≤ 42°N).

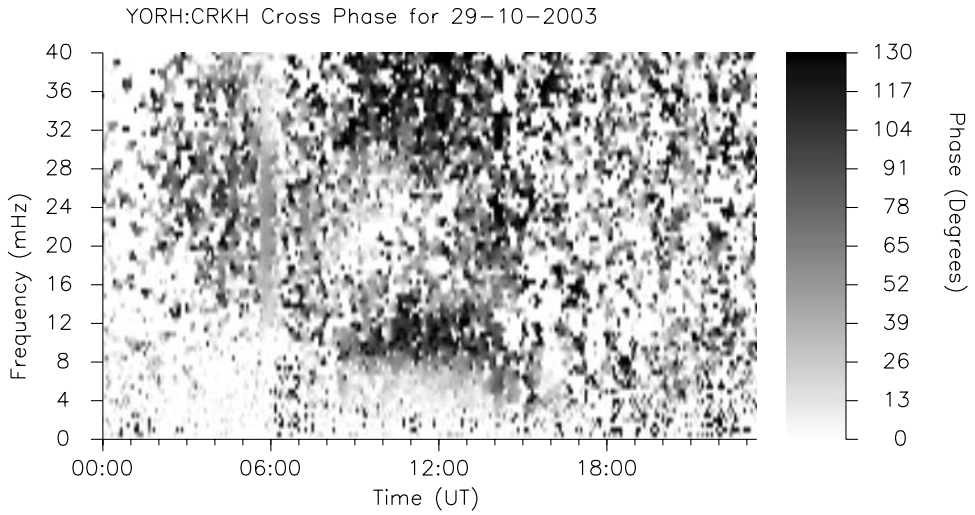

Figure 5. Dynamic cross-phase spectra for the YOR-CRK station pair (magnetic latitude = 53°N) for 29 October 2003. A similar diurnal trend was shown in dynamic cross-phase spectra from all of the SAMNET station pairs (49°N ≤ magnetic latitude ≤ 63°N).

until the second SSC occurs. There is also a diurnal variation of the frequencies with lower frequencies in the afternoons.

[13] Figures 4 and 5 show example dynamic cross-phase spectra for 29 October 2003, which are representative of the spectra calculated using data from the other station pairs in the SEGMA and SAMNET arrays, respectively, for that day. Field-line resonance frequencies are shown by enhanced cross-phase values. After the 0611 UT SSC, Figure 4 shows the first two harmonics.

[14] Figure 6 shows the plasma mass density values determined from these frequencies, using the method described above. No density values are shown where the T01 model calculated an "open" field line. Error bars have been omitted from these figures for clarity, although the mean error associated with the frequency values in Figure 3 is ±2.1 mHz. This error represents the uncertainty associated with determining the field line resonance frequencies. The two dashed vertical lines in each plot show the times of the SSCs which occurred during this interval (see Figure 2). Note that density decreases with increasing latitude, and the diurnal trends of each flux tube mirror the frequency trends shown in Figure 3. Day-to-day density variations show the storm-time plasmaspheric dynamics during this interval. Figure 7 shows the T01 derived field line apex location, in units of R_E, as a function of time. Field line resonances are most sensitive to the plasma mass density where the Alfvén speed is small, and for a given field line this occurs at the furthest distance from Earth, the "apex". This plot of apex location gives an indication as to whether these field

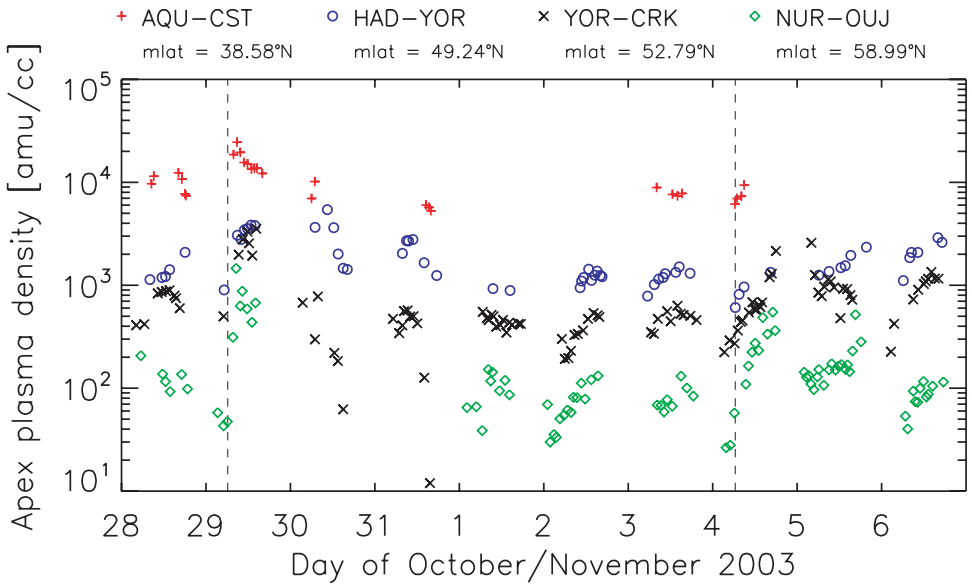

Figure 6. Cross-phase determined T01 field line apex plasma mass densities for four flux tubes for 28 October−6 November 2003 (AQU-CST, HAD-YOR, YOR-CRK, and NUR-OUJ). Dashed vertical lines have been placed at the UT of the two SSCs occurring during this interval. See text for details.

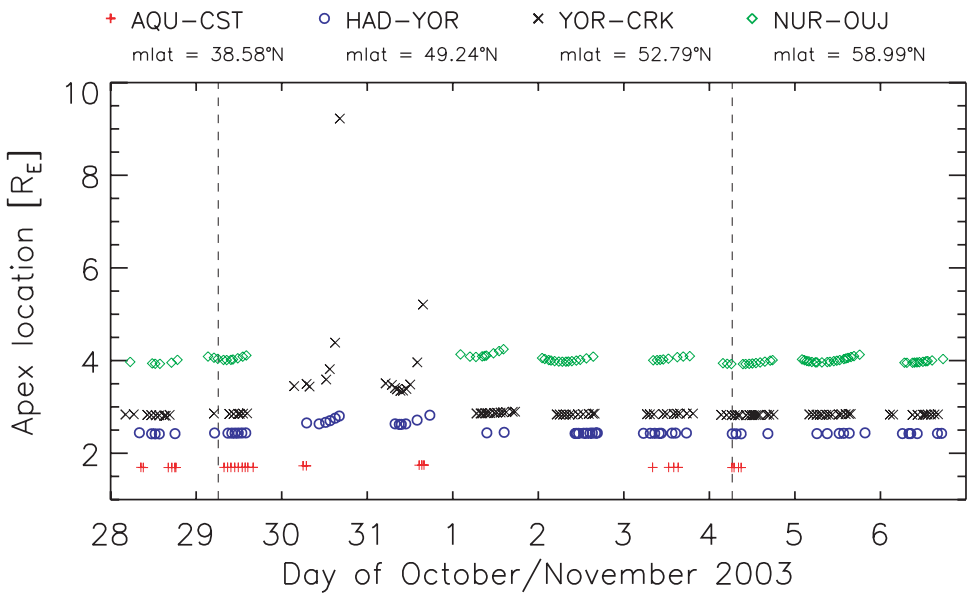

Figure 7. T01 derived apex location for four field lines for 28 October–6 November 2003 (AQU-CST, mlat = 38.58°N; HAD-YOR, mlat = 49.24°N; YOR-CRK, mlat = 52.79°N; NUR-OUJ, mlat = 58.99°N). Dashed vertical lines have been placed at the UT of the two SSCs occurring during this interval.

lines were stretching or contracting throughout the storm interval. Equatorward of 50°N mlat, only modest variations in apex location occurred, but poleward of 50° mlat, significant stretching occurred during the storm main phase.

[15] Figure 8 shows the variation of field line resonance frequency with magnetic latitude, as monitored for 28 October–6 November by the thirteen station pairs listed in Table 1. Again, the resonance frequencies were determined using Fourier transform data windows between 20 and 50 minutes duration, and were centred on 0930 UT ± 1 hour. Note that a resonance frequency value was unable to be determined for every station pair at this UT every day. This in itself may be an important feature as cross-phase peaks may be suppressed at the plasmapause or other large density discontinuities [e.g., *Milling et al.*, 2001]. Figure 9 shows the plasma mass density profiles determined from these resonance frequency values, using the method described above. The left column plots density versus magnetic latitude, in order to highlight the variations observed from day to day by each station pair. The right hand column plots plasma mass density versus apex location in order to highlight the effect of field line stretching on the density profile as it would be observed in situ. No density values are shown where the T01 model calculated an "open" field line. For clarity, error bars have only been added to one profile in each panel, and the latter profile from the previous panel is repeated in each subsequent panel to aid day-to-day comparison.

4. Discussion

4.1. Post-SSC Resonant Frequency Decrease

[16] Figure 3 shows that shortly after the SSC on 29 October, a sharp decrease of field line resonance frequency occurred at the three midlatitude field lines monitored (HAD-YOR, YOR-CRK, and NUR-OUJ). Although an accurate field line resonance frequency could not be determined for the low-latitude AQU-CST station pair immediately prior to the SSC, a sharp decrease of frequency of the cross-phase peak in the dynamic spectrogram (Figure 4) is clear after the SSC (until around 0800 UT). A similar trend is also present in the dynamic cross-phase spectra between the other pairs of the low latitude SEGMA magnetometer station pairs examined (not shown). Figure 5 shows the resonance frequency decrease monitored by the YOR-CRK station pair following the SSC.

[17] Figure 3 shows that the low latitude station pair, AQU-CST, monitored a subsequent increase in resonance frequency, f_r, (and a decrease in density, Figure 6) through the day following this initial SSC related f_r decrease. The same rise of f_r is clear in the dynamic cross-phase spectra of all six low latitude (SEGMA) station pairs (not shown). In contrast, the three midlatitude station pairs demonstrated a continued decrease of frequency (and a increase in density) as the day progressed. This implies that the midlatitude flux tubes monitored by the SAMNET stations were in general undergoing different physical processes than the lower latitude flux tubes monitored by the low-latitude SEGMA stations; or the cause of the sharp field line resonance frequency decrease could have been the same at all latitudes, but was shorter lived at the lower latitudes.

[18] A decrease of field line resonance frequency is caused either by an enhancement of density, or field-line lengthening. During the course of a severe geomagnetic storm when the magnetospheric cavity is compressed, field-line lengthening is unlikely unless the ring current penetrates to low L shells, and Figure 7 shows that is unlikely to have occurred in that region on 29 October. An increase of plasma mass density is in fact shown in Figure 6. The rate of density increase shown in Figure 6 was as high as 965 amu/cc/hour. Such an increase of plasma mass density may be achieved by up-flowing O^+ ions from the ionosphere. *Fraser et al.* [2005] showed that O^+ ions may be enhanced in the vicinity of the plasmapause following a storm onset.

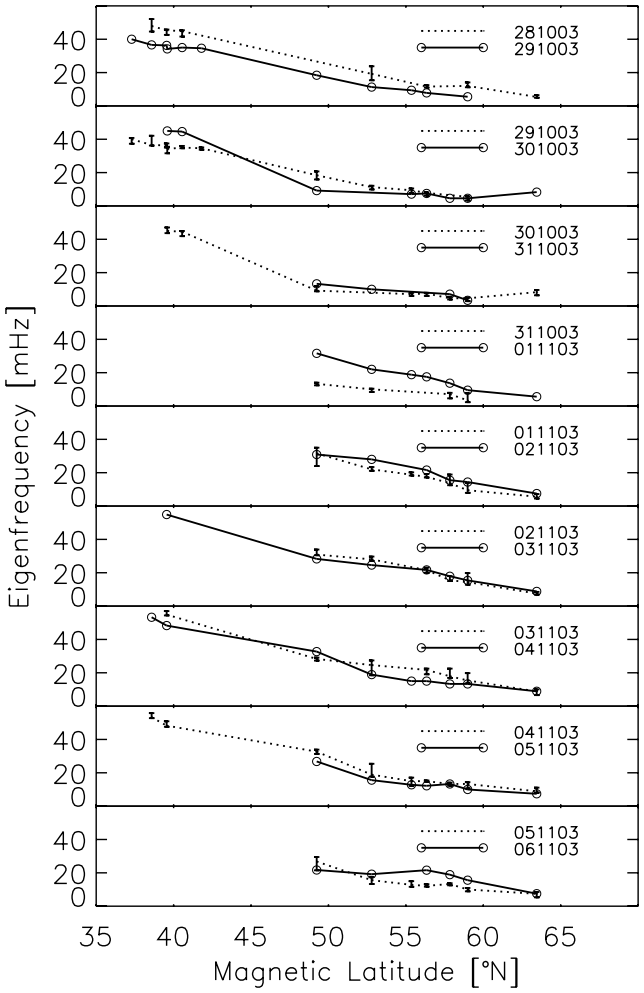

Figure 8. Daily field line resonance frequency profiles for 0930 UT. Two profiles are shown in each plot, with profiles repeated in consecutive panels for easier comparison. Error bars have been added to the earlier of the two profiles in each panel and represent the uncertainty associated with determining each resonance frequency using the cross-phase technique. Data points have been joined to guide the eye.

Allan [1993] suggest that the pondermotive force may accelerate ionospheric particles toward the equatorial plane, the acceleration increasing with L shell and particle mass, i.e. O^+ ions would undergo the greatest acceleration and hence outflow. An alternative mechanism was offered by *Yeh and Foster* [1990], who examined Millstone Hill incoherent scatter radar observations in the dusk sector during the course of a severe geomagnetic storm, and observed an enhanced O^+ outflow for over four hours during the storm event. *Yeh and Foster* concluded that the combined effects of ring current ion precipitation and rapid ion convection could explain their observation, and that under such conditions the resulting ionospheric heating could represent a significant source of magnetospheric thermal O^+ ions. Also, O^+ upflow may be caused in auroral regions, which extended to low latitudes for this event [e.g., *Stevenson et al.*, 2001; *Tóth et al.*, 2007].

[19] *Chi et al.* [2005] monitored plasma mass density along a meridian spanning $2.4 \leq L \leq 9.5$ in the North American sector (LT = UT − 6.3 hours) throughout this Hallowe'en event. They also found a significant density enhancement on 29 October, peaking at four to five times larger than the typical density on 30 October. This shows that this density enhancement was not a highly localized effect, limited to a specific meridian or local time sector. *Chi et al.* compared their results to those of Total Electron Content (TEC) up to ~20 000 km, which showed tongues of ionization in the region where the enhanced plasma mass density was observed. They therefore suggested that plasmaspheric drainage plumes were being monitored, but noted that the density enhancement occurred unusually quickly, and also discussed the possibility of O^+ rich outflow from the ionosphere, or an inner ionospheric source of dense plasma as being possible causes. Figure 3 of *Chi et al.* shows a density increase between 00 UT and 12 UT (local nightside sector) on 29 October, which did not correspond to an increase in TEC, so is suggestive of an enhanced heavy ion population. The observations presented here suggest O^+ outflow played an important role in total mass density dynamics during this storm, especially at midlatitudes.

[20] *Takasaki et al.* [2006] also studied this event at low latitudes ($L \sim 1.4$) using ground-based magnetometer data from Japan (LT = UT + 9 hours). While they did not monitor a significant decrease of field-line resonant frequency on 29 October (in fact they did not present data for 29 October following the SSC at 0611 UT), they did monitor a large decrease of frequency (increase of mass density) below quiet-day values following the large decrease of Dst early on 31 October. The TEC value for that region was close to quiet time values, leading *Takasaki et al.* to suggest that an up-flow of O^+ ions from the ionosphere was the cause, consistent with our interpretation on higher latitude field-lines at earlier times. The *Takasaki et al.* density increase at $L \sim 1.4$ persisted for only a few hours, and this was explained in terms of a combination of the O^+ enhancement and plasmaspheric erosion, or due to the effect of gravity.

[21] The profile plots (Figures 8 and 9) show that the decrease of resonance frequency (increase of plasma mass density) between 28 and 29 October (both monitored at 0930 UT) was observed at all magnetic latitudes between 40° and 59°N (low- to midlatitudes).

[22] Collectively, these observations of enhanced mass density occurring on different days along different meridians during this storm interval suggest that there can be a delicate competition between density enhancements from heavy ion up-flow from the ionosphere and losses creating plasmaspheric density decreases generating a response which can have structure and variation with local time and UT.

[23] *Dent et al.* [2006] monitored enhanced mass density in a region of unchanging electron number density, following a Dst decrease beginning at ~1900 LT the previous day, consistent with O^+ outflow. The observations of enhanced mass density mentioned above occurred following a decrease of Dst which began between 1900 LT and 0900 LT (i.e., the night-side sector). The day-side sector (~0900–1900 LT) is where plasmaspheric plasma is convected

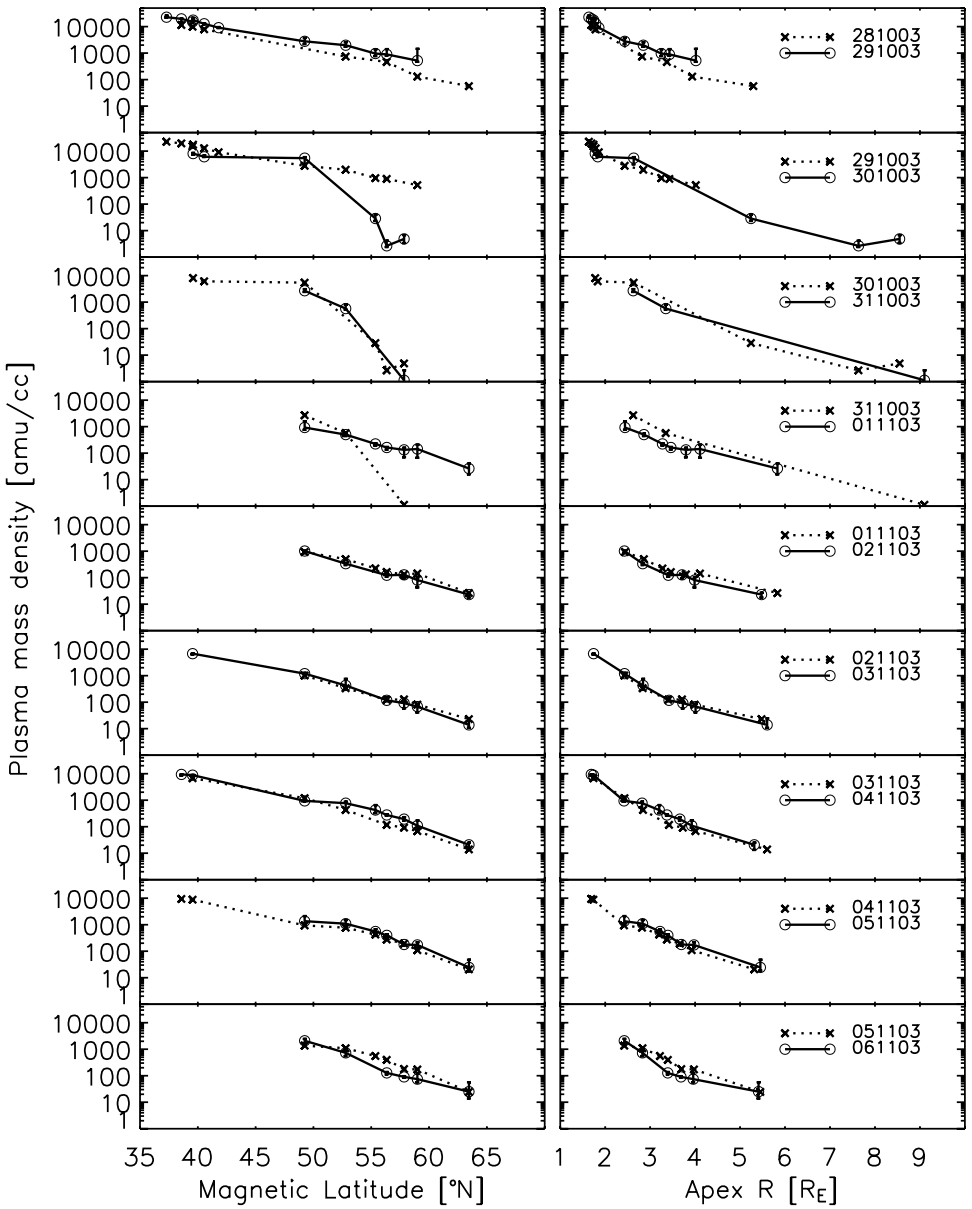

Figure 9. Daily plasma mass density profiles for 0930 UT. The left-hand column plots density as a function of station pair midpoint magnetic latitude, and the right-hand column plots density as a function of field line apex location. Profiles are plotted similarly to Figure 8, and error bars shown are those calculated using the uncertainty associated with the resonance frequency values. Data points have been joined to guide the eye.

sunward during geomagnetic storms, so it is plausible that any O^+ up-flow from the ionosphere occurring in this local time sector following a SSC would not be monitored as a mass density increase.

[24] In addition to plume formation, other possible scenarios which would explain a rapid enhancement of plasma mass density are plasmaspheric compression [e.g., *Tsurutani et al.*, 2004], outflow arising from lifting of the ionosphere F layer to a region of reduced recombination during the storm main phase [e.g., *Soicher*, 1976], or convection of dense flux tubes with low latitude footprints into the field of view of higher latitude station pairs. None of these processes would cause an increase in the proportion of heavy ions, as shown by *Takasaki et al.* [2006] and *Chi et al.* [2005], however. It is of course possible that more than one process was in effect. Clearly more observations of ion populations and/or coordinated studies of plasma mass density and electron number density, for example, are required to better understand the local time effects of geomagnetic storm related mass density enhancements and the balance between heavy ion outflow and convective flux tube dynamics.

4.2. Plasmaspheric Density Depletion

[25] Figures 6 and 9 show plasma density values decreasing following the geomagnetic storm of 29 October. This plasmaspheric erosion continued until 31 October.

[26] In their ISEE study of electron number density, *Carpenter and Anderson* [1992] estimated that a well

defined plasmapause should appear locally in the late afternoon-dusk sector approximately 10 hours after the beginning of the convection episode causing the depletion. This is a much shorter timescale than shown in Figure 6. *Baker et al.* [2004] presented some IMAGE satellite EUV images of the plasmaspheric He^+ population for this Hallowe'en 2003 interval. Although images were not presented for every day throughout the storm, they clearly observed a globally depleted plasmasphere by 0138 UT on 31 October; with the He^+ plasmapause laying inside 2 R_E, and a plasmaspheric drainage plume clearly present in the afternoon sector. This is in reasonable agreement with our plasma density profiles for 30 October (Figure 9, right hand column), which shows a plasmapause, defined in terms of total mass density, around 2.6 R_E.

[27] Note that no field line resonance frequencies were obtained for the profile plots at lower latitude station pairs (mlat $\leq$ 42°N) between 31 October and 2 November. A suppression of the cross-phase peak may be indicative that these station pairs were in the vicinity of the plasmapause or some other steep plasma density gradient throughout this interval [see *Milling et al.*, 2001], consistent with the *Baker et al.* [2004] IMAGE EUV images.

4.3. Field Line Distortion

[28] Figure 7 shows that for eight of the ten days studied, only the highest latitude station pair (NUR-OUJ, mlat = 58.99°N) shows regular diurnal field line stretching along the dawn and dusk flanks, with a minimum apex location across the noon meridian [see *Waters et al.*, 1995]. Moreover, on 30 and 31 October a significant amount of field-line stretching took place along field lines with footprints at mlat $\geq$ 49°N (i.e., poleward of HAD-YOR), as indicated by the increase of apex location value (Figure 7). This field line stretching occurred during the two days following the first SSC, when |Dst| was large and also when plasma mass density was decreasing (Figure 6). The stretching became more severe in the local afternoon sector, consistent with penetration of the partial ring current. Field line stretching and plasma depletion taking place simultaneously is an entirely expected scenario in the context of a penetrating ring current and plasmaspheric drainage plumes.

[29] Figure 9 shows plasma density depletion at magnetic latitudes $\geq$ 50°N between 29 and 30 October, and as discussed above, this is likely to be due to the field line stretching as calculated by the T01 model causing an increased flux tube volume. However, it is entirely possible that additional plasma loss also occurred along these flux tubes.

[30] Note that if plasma density is derived assuming a dipolar magnetic field geometry, then the density enhancement monitored immediately following the SSC appears to be maintained through 30 and 31 October, with no diurnal density decreases monitored through these days.

4.4. Drainage Plume

[31] The diurnal trend monitored on 1 November (Figures 3 and 6), which Figure 2 shows is the first geomagnetically quiet day after the first SSC, does not show typical refilling. The NUR-OUJ (mlat = 58.99°N) station pair monitors a decrease followed by an increase of density through the day, consistent with the field-line encountering the remnants of the plasmaspheric drainage plume.

4.5. Plasmaspheric Refilling

[32] Figure 6 shows that by 2 November the diurnal density variations reached a minimum early morning value at the YOR-CRK and NUR-OUJ station pairs (mlat = 52.79 and 58.99°N respectively). This shows that storm-time depletion was complete, with diurnal refilling both increasing plasma mass density through the course of each day, but also resulting in a gradual density increase from day to day. Indeed, Figure 9 shows no noticeable decrease of density between 2 and 3 November at 0930 UT. At that time there were significant diurnal variations with night-side depletions occurring in addition to the day-side refilling.

4.6. Early Morning Frequency Maxima

[33] On 2 November, Figure 3 shows a sharp increase of field line resonance frequency early in the morning, monitored by the YOR-CRK and NUR-OUJ station pairs. Figure 6 shows a corresponding sharp density decrease derived from these values and Figure 7 shows no significant change in the field line apex locations during this interval. The early morning very low value of resonance frequency may be attributed to a quarter-wave mode standing Alfvén wave, which can occur when the footprints of a field line are either side of the dawn terminator. Such a scenario is described in detail by *Obana et al.* [2008].

4.7. Density Dynamics Following the Second SSC

[34] At 0625 UT on the 4 November the second SSC occurred, and the geomagnetic indices plotted in Figure 2 show that the disturbance this produced was less severe, and shorter-lived, than that following the SSC on 29 October. One very interesting feature on this day is the large range of resonant frequencies (and plasma mass densities) monitored, particularly by YOR-CRK (mlat = 52.79°N) and NUR-OUJ (mlat = 58.99°N) data (Figure 3). The resonant frequency decrease at midlatitudes is similar to that shown for 29 October in Figures 3 and 6. On 29 October the decrease of field line resonance frequency occurred rapidly, followed by a slower diurnal increase monitored by the lowest latitude station pair, and further slower diurnal decrease monitored by the higher midlatitude station pairs. On 4 November, however, the field line resonance frequency decreased more gradually following the SSC and with a clear, if less steep, continued decrease throughout the rest of the daytime observations by the three higher midlatitude station pairs in Figure 6. As with the 29 October SSC, the behavior of resonance frequency immediately following the 4 November SSC could indicate an enhancement of the heavy ion, possibly O^+, population throughout 4 November. Alternatively, these station pairs may have monitored dense plasmaspheric plasma in the day-side sector as it convected sunward. No IMAGE EUV images are available for 4 November 2003 after the SSC at 0625 UT, so this plume scenario cannot be investigated further.

[35] Figure 3 shows that an overall decrease of frequency (corresponding to an increase of density, Figure 6) through 5 November was monitored by the HAD-YOR (mlat = 49.24°N) and NUR-OUJ (mlat = 58.99°N) station pairs.

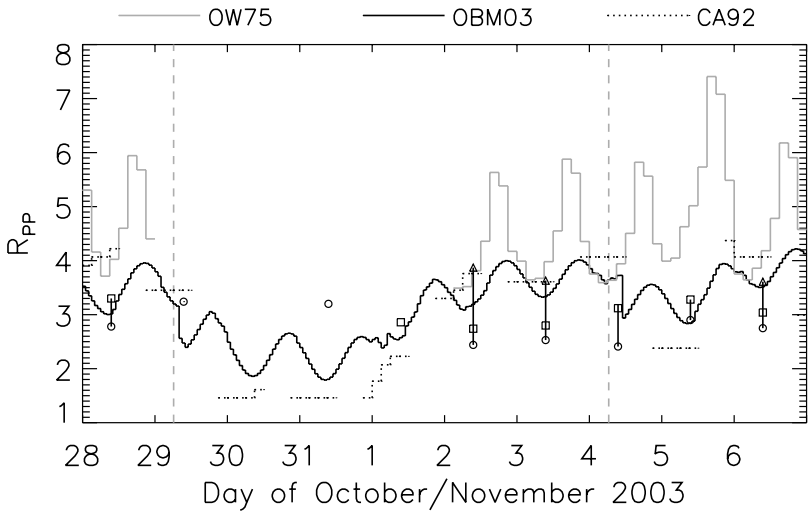

Figure 10. Empirical plasmapause model predictions versus universal time for 28 October–6 November 2003. Predictions shown are from the local time dependent, Kp-driven [*Orr and Webb*, 1975] model [OW75]; the magnetic local time-dependent, Dst-driven [*O'Brien and Moldwin*, 2003] model [OBM03]; and the non-local time dependent, Kp-driven [*Carpenter and Anderson*, 1992] model [CA92]. The location of 1000, 500, and 100 amu/cc density values along each profile presented in Figure 9 are shown by open circles, squares, and triangles, respectively. Vertical dotted lines have been placed at the UT of the two SSCs, which occurred during this interval.

At YOR-CRK (mlat = 52.79°N) an overall increase of frequency was monitored. Such a variation of plasma mass density with L shell and time may be explained by the presence of a residual drainage plume or other azimuthal asymmetry of the plasmapause being monitored by YOR-CRK.

[36] Figure 9 shows that plasma depletion at 56°N $\leq$ mlat $\leq$ 59°N (YOR-CRK–NUR-OUJ) occurred between 5 and 6 November. This is due to enhanced convection associated with the storm following the SSC on 4 November.

4.8. Empirical Plasmapause Models

[37] In order to gain a better understanding of the plasmaspheric morphology and dynamics which explain the observed density increases immediately following the SSCs for these Hallowe'en storms, and in the absence of electron number density observations (no suitable in situ satellite observations of electron number density have been found for this event), empirical plasmapause models have been employed. These will show the statistical expectation of the plasmapause location through the interval of interest, and can be compared with our observations.

[38] Figure 10 shows predicted radial plasmapause location (R_{pp}, in units of R_E) versus UT, and for the central meridian (in LT, or MLT, as appropriate for each model) monitored by the magnetometers employed. The *Carpenter and Anderson* [1992] (CA92) model is driven by the Kp index, using the maximum Kp value which occurred in the preceding 24 hours, excluding some local morning hours. This model is valid for 0000 $\leq$ MLT $\leq$ 1500, and is not limited during high or low Kp intervals. The *O'Brien and Moldwin* [2003] (OBM03) model is driven by the Dst index, using the maximum Dst value occurring during the preceding 24 hours. It is valid for Dst ≤ -2 nT and is MLT dependent. The *Orr and Webb* [1975] (OW75) model is Kp driven, using the average Kp value for the preceding local nighttime sector. It offers local time variation but is limited to average Kp values less than 4. The local and magnetic local time variations are clear in the OW75 and OBM03 R_{pp} variations in Figure 10. All models predict the L shell of the plasmapause location. Also plotted are the 1000, 500 and 100 amu/cc density locations, linearly interpolated from cross phase values plotted in Figure 9. In order to minimize uncertainty, where the radial sepatation between data points is greater than 1 R_E, or the density difference between two cross phase points is greater than one order of magnitude, an interpolation has not been carried out. This range of values typically identifies and spans density values which characterize the plasmapause region [e.g., *Dent et al.*, 2006]. The separation of the symbols representing these three density values at each UT indicates how shallow or steep the plasmapause profile is. However, the spatial resolution in Figure 9 arising from available station pair sampling, may cause the plasmapause gradient to appear smoothed. Also, note that the OBM03 and CA92 models were developed using data comprised only of observed steep plasmapause profiles, so would not be expected to successfully predict the plasmapause location on those days when a shallow plasmapause profile is observed. In contrast, the OW75 model was developed using observations of the 10 H^+ ions per cc location.

[39] The OW75 model is invalid for most of 29 October–1 November. The OBM03 and CA92 models, however, show a statistical expectation of an inward motion of the plasmapause, of 0.6 R_E immediately following the SSC on 29 October, and a total of 2 R_E by 30 October, respectively (compared to the prestorm plasmapause locations). There is no similar trend in the limited cross-phase-derived data for this period; the 1000 amu/cc density location is at the same radial location on 31 October as 29 October. The models did not take account of heavy ions, so this disparity could add

weight to the hypothesis of enhanced O^+ during this interval. Note, however that Figures 9 and 6 do not show a similar density depletion through 29 and 30 October. Density depletion is shown in these figures to have occurred by 1 November, more than one day after the empirical model predictions.

[40] The OBM03 and CA92 models predict an outward moving plasmapause between 31 October and 2 November, by $\sim$1.7 and >2 R_E, respectively (measured between the maximum R_{pp} location on each day). This would indicate refilling taking place along field lines inward of the predicted plasmapause location. The cross-phase-derived 1000 and 500 amu/cc locations move inward through this interval, suggesting depletion was taking place, or at least stretched field lines were relaxing back to a more dipolar geometry (Figure 7). It is clear from our results that overall a net increase in day-to-day density due to refilling does not occur until 2 November, one day after the empirical models' predictions. However, by 2 November the empirical models are in good agreement with the cross-phase-derived 500–100 amu/cc location.

[41] On 4 November the distance between the 1000 and 500 amu/cc locations indicates a shallower density gradient than during the preceding two days. This occurred after the SSC and approximately when the CA92 and OBM03 models predict a sharp inward movement of the plasmapause. This shallower density gradient could be due to the suspected upflowing of heavy ions, or could be a result of the poststorm refilling which took place during the preceding two days.

[42] The OW75 model predicts a slight inward motion of the plasmapause between 5 and 6 November. This is in response to the enhanced Kp index late on 5 November, not the enhanced levels on 4 November. However, this prediction of the OW75 model does imply plasma loss and is consistent with the observation of plasma depletion at $3 \lesssim$ apex $R \lesssim 4$ between 5 and 6 November (Figure 9). The CA92 and OBM03 models predict an outward moving plasmapause between 5 and 6 November, an opposite trend to the cross-phase-derived (inward) trend.

[43] Generally, the OBM03 and CA92 models have good coverage throughout the storm interval, whereas the OW75 model was less useful for interpretation since it was invalid throughout the storm main and early recovery phases. The innermost model predicted plasmapause locations on 1 November of $R_{pp} \leq 2$ is slightly inward of cross-phase-derived depletion to $R \gtrsim 2.6$, as shown in Figure 9. The CA92 and OBM03 models tend to successfully predict the observed trends of plasmapause motion in response to plasmaspheric depletion and refilling, albeit approximately one day prematurely.

5. Conclusion

[44] This study presents ground-based magnetometer derived observations of plasma mass density dynamics between magnetic latitude = 37°N and 63°N for 28 October–6 November 2003, the "Hallowe'en" storm interval. Immediately following the SSC on 29 October a plasma mass density increase occurred at all latitudes monitored, probably due to up-flowing O^+ ions from the ionosphere. A similar plasma mass density trend was also observed following the SSC on 4 November, and O^+ ions are also suggested to be the cause.

[45] IMAGE EUV images presented by *Baker et al.* [2004] show a depletion of the He^+ plasmaspheric population by early on 31 October, in agreement with the plasma mass density dynamics presented here. This study further emphasizes the importance of choosing an appropriate geomagnetic field line model when deriving plasma mass densities from ground-based magnetometer derived field line eigenfrequencies.

[46] The location of the plasmapause throughout a storm interval is considered to be of increasing importance for radiation belt dynamics. There is evidence that the inner edge of the outer zone Van Allen electron radiation belt is well correlated with the position of the plasmapause [e.g., *Baker et al.*, 2004]. Explanations may include the effect of electron density and plasmapause location control of the mass density on the penetration of ULF waves [*Loto'aniu et al.*, 2006] or the effectiveness of VLF wave-particle interactions [e.g., *Blanc et al.*, 1999], respectively, which may be involved in radiation belt acceleration.

[47] In terms of examining the diurnal variation of mass density, an early morning minima was monitored by two station pairs on 2 November, the first day of poststorm refilling. This may be the result of one field line ionospheric footprint being sunlit while the other is in darkness, causing a quarter-wave mode.

[48] Overall, the results presented here demonstrate the powerful capability of employing ULF waves monitored by ground-based magnetometers in order to study plasma mass dynamics in the storm-time magnetosphere. During the Hallowe'en study interval, there is evidence for a rapid injection of heavy, presumably O^+, ions from the ionosphere to the magnetosphere on timescales of $\sim$1 hour. Given the importance of both total mass and electron density profiles in the inner magnetosphere for ULF or VLF MeV electron acceleration, and indeed in controlling the dispersion relation of electromagnetic ion cyclotron EMIC waves believed to be important for MeV electron loss, understanding total mass as well as heavy ion and electron density dynamics during storms is likely to be of considerable importance. ULF wave cross-phase monitoring from networks of ground-based magnetometers can contribute significantly to such studies.

[49] **Acknowledgments.** Z.C.K. thanks F.W. Menk for cross-phase analysis tools and L.G. Ozeke for the dipole model density inversion program. BGS is a NERC funded facility, and SAMNET is operated by Lancaster University and funded by STFC. We thank the SAMNET team for providing the SAMNET and BGS magnetometer data. We thank N.F. Ness for the ACE MAG data; D. J. McComas, Ruth Skoug, and the ACE/SWEPAM team for the ACE SWEPAM data; the World Data Center for Geomagnetism, Kyoto for Dst and Kp indices; NSSDCWeb for MLT calculations; OMNIWeb for Tsyganenko 01 model input parameters; National Geophysical Data Center for SSC information; and the U.S. Naval Observatory for sunrise information. This work was supported by a Discovery Grant from NSERC of Canada to IRM and also by the CSA.

[50] Amitava Bhattacharjee thanks Joseph Lemaire and another reviewer for their assistance in evaluating this paper.

References

Allan, W. (1993), The ponderomotive force of standing Alfvén waves in a dipolar magnetosphere, *J. Geophys. Res.*, *98*(A2), 1409–1417.

Baker, D. N., S. G. Kanekal, X. Li, S. P. Monk, J. Goldstein, and J. L. Burch (2004), An extreme distortion of the Van Allen belt arising from the "Hallowe'en" solar storm in 2003, *Nature*, *432*(7019), 878–881.

Baransky, L. N., S. P. Belokris, Y. E. Borovkov, M. B. Gokhberg, E. N. Federov, and C. A. Green (1989), Restoration of the meridional structure of geomagnetic pulsation fields from gradient measurements, *Planet. Space Sci.*, *37*(7), 859–864.

Baumjohann, W., and R. A. Treumann (1999), *Basic Space Plasma Physics*, Imperial College Press, London, U. K.

Blanc, M., J. L. Horwitz, J. B. Blake, I. Daglis, J. F. Lemaire, M. B. Moldwin, S. Orsini, R. M. Thorne, and R. A. Wolfe (1999), Source and loss processes in the inner magnetosphere, *Space Sci. Rev.*, *88*(1–2), 137–206.

Carpenter, D. L., and R. R. Anderson (1992), An ISEE/whistler model of equatorial electron density in the magnetosphere, *J. Geophys. Res.*, *97*(A2), 1097–1108.

Chi, P. J., C. T. Russell, S. Musman, W. K. Paterson, G. Le, V. Angelopolous, G. D. Reeves, M. B. Moldwin, and F. K. Chun (2000), Plasmaspheric depletion and refilling associated with the September 25, 1998 magnetic storm observed by ground magnetometers at L = 2, *Geophys. Res. Lett.*, *27*(5), 633–636.

Chi, P. J., C. T. Russell, J. C. Foster, M. B. Moldwin, M. J. Engebretson, and I. R. Mann (2005), Density enhancement in plasmasphere-ionosphere plasma during the 2003 Halloween Superstorm: Observations along the 330th meridian in North America, *Geophys. Res. Lett.*, *32*, L03S07, doi:10.1029/2004GL021722.

Comfort, R. H., I. T. Newberry, and C. R. Chappell (1988), Preliminary statistical survey of plasmaspheric ion properties from observations by DE1/RIMS, in *Modeling Magnetospheric Plasma*, *Geophys. Monogr. Ser.*, vol. 44, edited by T. E. Moore and J. H. Waite Jr., pp. 107–114, AGU, Washington, D. C.

Dent, Z. C., I. R. Mann, J. Goldstein, F. W. Menk, and L. G. Ozeke (2006), Plasmaspheric depletion, refilling and plasmapause dynamics: A coordinated ground-based and IMAGE satellite study, *J. Geophys. Res.*, *111*, A03205, doi:10.1029/2005JA011046.

Fraser, B. J., J. L. Horwitz, J. A. Slavin, Z. C. Dent, and I. R. Mann (2005), Heavy ion mass loading of the geomagnetic field near the plasmapause and ULF wave implications, *Geophys. Res. Lett.*, *32*, L04102, doi:10.1029/2004GL021315.

Goldstein, J., M. Spasojević, P. H. Reiff, B. R. Sandel, T. Forrester, D. L. Gallagher, and B. W. Reinisch (2003), Identifying the plasmapause in IMAGE EUV data using IMAGE RPI in situ steep density gradients, *J. Geophys. Res.*, *108*(A4), 1147, doi:10.1029/2002JA009475.

Horwitz, J. L., R. H. Comfort, and C. R. Chappell (1984), Thermal ion composition measurements of the formation of the new outer plasmasphere and double plasmapause during storm recovery phase, *Geophys. Res. Lett.*, *11*(8), 701–704.

Hughes, W. J. (1974), The effect of the atmosphere and ionosphere on long period magnetospheric micropulsations, *Planet. Space Sci.*, *22*, 1157–1172.

Lemaire, J. F., K. I. Gringauz, D. L. Carpenter, and V. Bassolo (1998), *The Earth's Plasmasphere*, Cambridge Univ. Press, Cambridge, U. K.

Loto'aniu, T. M., I. R. Mann, L. G. Ozeke, A. A. Chan, Z. C. Dent, and D. K. Milling (2006), Radial diffusion of relativistic electrons into the radiation belt slot region during the 2003 Halloween geomagnetic storms, *J. Geophys. Res.*, *111*, A04218, doi:10.1029/2005JA011355.

Menk, F. W., D. Orr, M. A. Clilverd, A. J. Smith, C. L. Waters, D. K. Milling, and B. J. Fraser (1999), Monitoring spatial and temporal variations in the dayside plasmasphere using geomagnetic field line resonances, *J. Geophys. Res.*, *104*(A9), 19,955–19,969.

Menk, F. W., C. L. Waters, and B. J. Fraser (2000), Field line resonances and waveguide modes at low latitudes: 1. Observations, *J. Geophys. Res.*, *105*(A4), 7747–7761.

Menk, F. W., I. R. Mann, A. J. Smith, C. L. Waters, M. A. Clilverd, and D. K. Milling (2004), Monitoring the plasmapause using geomagnetic field line resonances, *J. Geophys. Res.*, *109*, A04216, doi:10.1029/2003JA010097.

Milling, D. K., I. R. Mann, and F. W. Menk (2001), Diagnosing the plasmapause with a network of closely spaced ground-based magnetometers, *Geophys. Res. Lett.*, *28*(1), 115–118.

Obana, Y., F. W. Menk, M. D. Sciffer, and C. L. Waters (2008), Quarter-wave modes of standing alfvén waves detected by cross-phase analysis, *J. Geophys. Res.*, *113*, A08203, doi:10.1029/2007JA012917.

O'Brien, T. P., and M. B. Moldwin (2003), Empirical plasmapause models from magnetic indices, *Geophys. Res. Lett.*, *30*(4), 1152, doi:10.1029/2002GL016007.

Orr, D., and D. C. Webb (1975), Statistical studies of geomagnetic pulsations with periods between 10 and 70 sec and their relationship to the plasmapause region, *Planet. Space Sci.*, *23*, 1169–1178.

Poulter, E. M., W. Allan, J. G. Keys, and E. Nielsen (1984), Plasmatrough ion mass densities determined from ULF pulsation eigenperiods, *Planet. Space Sci.*, *32*(9), 1069–1078.

Sandel, B. R., R. A. King, W. T. Forrester, D. L. Gallagher, A. L. Broadfoot, and C. C. Curtis (2001), Initial results from the IMAGE Extreme Ultraviolet Imager, *Geophys. Res. Lett.*, *28*(8), 1439–1442.

Sandel, B. R., J. Goldstein, D. L. Gallagher, and M. Spasojević (2003), Extreme UltraViolet imager observations of the structure and dynamics of the plasmasphere, *Space Sci. Rev.*, *109*, 25–46.

Singer, H. J., D. J. Southwood, R. J. Walker, and M. G. Kivelson (1981), Alfvén wave resonances in a realistic magnetospheric magnetic field geometry, *J. Geophys. Res.*, *86*(A6), 4589–4596.

Skoug, R. M., J. T. Gosling, J. T. Steinberg, D. J. McComas, C. W. Smith, N. F. Ness, Q. Hu, and L. F. Burlaga (2004), Extremely high speed solar wind: 29–30 October 2003, *J. Geophys. Res.*, *109*, A09102, doi:10.1029/2004JA010494.

Soicher, H. (1976), Response of electrons in ionosphere and plasmasphere to magnetic storms, *Nature*, *259*, 33–35.

Stevenson, B. A., J. L. Horwitz, G. Germany, T. E. Moore, B. L. Giles, P. D. Craven, M. O. Chandler, Y.-J. Su, and G. K. Parks (2001), Polar observations of topside field-aligned O^+ flows and auroral forms, *J. Geophys. Res.*, *106*(A9), 18,969–18,979.

Takasaki, S., H. Kawano, Y. Tanaka, A. Yoshikawa, M. Seto, M. Iizima, Y. Obana, N. Sato, and K. Yumoto (2006), A significant mass density increase during a large magnetic storm in October 2003 obtained by ground-based ULF observations at L $\sim$ 1.4, *Earth Planets Space*, *58*, 617–622.

Tóth, G., D. L. De Zeeuw, T. I. Gombosi, W. B. Manchester, A. J. Ridley, I. V. Sokolov, and I. I. Roussev (2007), Sun-to-thermosphere simulation of the 28–30 October 2003 storm with the Space Weather Modeling Framework, *Space Weather*, *5*, S06003, doi:10.1029/2006SW000272.

Tsurutani, B., et al. (2004), Global dayside ionospheric uplift and enhancement associated with interplanetary electric fields, *J. Geophys. Res.*, *109*, A08302, doi:10.1029/2003JA010342.

Tsyganenko, N. A. (2002a), A model of the near magnetosphere with a dawn-dusk asymmetry: 1. Mathematical structure, *J. Geophys. Res.*, *107*(A8), 1179, doi:10.1029/2001JA000219.

Tsyganenko, N. A. (2002b), A model of the near magnetosphere with a dawn-dusk asymmetry: 2. Parameterization and fitting to observations, *J. Geophys. Res.*, *107*(A8), 1176, doi:10.1029/2001JA000220.

Vellante, M., and M. Förster (2006), Inference of the magnetospheric plasma mass density from field line resonances: A test using a plasmasphere model, *J. Geophys. Res.*, *111*, A11204, doi:10.1029/2005JA011588.

Vellante, M., et al. (2004), Ground/satellite signatures of field line resonance: A test of theoretical predictions, *J. Geophys. Res.*, *109*(A6), A06210, doi:10.1029/2004JA010392.

Villante, U., P. Francia, M. Vellante, and P. Di Guiseppe (2003), Some aspects of the low latitude geomagnetic response under different solar wind conditions, *Space Sci. Rev.*, *107*, 207–217.

Waters, C. L., F. W. Menk, and B. J. Fraser (1991), The resonance structure of low latitude Pc3 geomagnetic pulsations, *Geophys. Res. Lett.*, *18*(12), 2293–2296.

Waters, C. L., F. W. Menk, and B. J. Fraser (1994), Low latitude geomagnetic field line resonance: Experiment and modeling, *J. Geophys. Res.*, *99*(A9), 17,547–17,558.

Waters, C. L., J. C. Samson, and E. F. Donovan (1995), The temporal variation of the frequency of high latitude field line resonances, *J. Geophys. Res.*, *100*(A5), 7987–7996.

Yeh, H.-C., and J. C. Foster (1990), Storm time heavy ion outflow at mid-latitude, *J. Geophys. Res.*, *95*(A6), 7881–7891.

Yeoman, T. K., D. K. Milling, and D. Orr (1990), Pi2 pulsation polarization patterns on the U.K. sub-auroral magnetometer network (SAMNET), *Planet. Space Sci.*, *38*(5), 589–602.

F. Honary, Department of Communication Systems, University of Lancaster, InfoLab21, Lancaster LA1 4WA, UK. (f.honary@lancaster.ac.uk)

Z. C. Kale and I. R. Mann, Department of Physics, University of Alberta, 11322-89 Avenue, Mail Stop #615, Edmonton, AB T6G 2G7, Canada. (zkale@phys.ualberta.ca; imann@phys.ualberta.ca)

M. Vellante, Dipartimento di Fisica, Università dell'Aquila, Via Vetoio Località Coppito, I-67100 L'Aquila, Italy. (massimo.vellante@aquila.infn.it)

C. L. Waters, School of Mathematical and Physical Sciences, University of Newcastle, Physics Building, University Drive, Callaghan, NSW 2308, Australia. (colin.waters@newcastle.edu.au)

T. L. Zhang, Space Research Institute, Austrian Academy of Sciences, Schmiedlestrasse 6, A-8042 Graz, Austria. (tielong.zhang@oeaw.ac.at)